doi:10.1093/brain/awv392 BRAIN 2016: 139; 782–794 | 782

BRAIN
A JOURNAL OF NEUROLOGY

LYRM7 mutations cause a multifocal cavitating leukoencephalopathy with distinct MRI appearance

Cristina Dallabona,[1,*] Truus E. M. Abbink,[2,*] Rosalba Carrozzo,[3,*] Alessandra Torraco,[3] Andrea Legati,[4] Carola G. M. van Berkel,[2] Marcello Niceta,[5] Tiziana Langella,[4] Daniela Verrigni,[3] Teresa Rizza,[3] Daria Diodato,[3] Fiorella Piemonte,[3] Eleonora Lamantea,[4] Mingyan Fang,[6,7] Jianguo Zhang,[6,7] Diego Martinelli,[8] Elsa Bevivino,[8] Carlo Dionisi-Vici,[8] Adeline Vanderver,[9] Sunny G. Philip,[10] Manju A. Kurian,[11,12] Ishwar C. Verma,[13] Sunita Bijarnia-Mahay,[13] Sandra Jacinto,[14] Fatima Furtado,[15] Patrizia Accorsi,[16] Anna Ardissone,[17] Isabella Moroni,[17] Ileana Ferrero,[1] Marco Tartaglia,[5] Paola Goffrini,[1] Daniele Ghezzi,[4,†] Marjo S. van der Knaap[2,†] and Enrico Bertini[3,†]

[*,†]These authors contributed equally to this work.

This study focused on the molecular characterization of patients with leukoencephalopathy associated with a specific biochemical defect of mitochondrial respiratory chain complex III, and explores the impact of a distinct magnetic resonance imaging pattern of leukoencephalopathy to detect biallelic mutations in *LYRM7* in patients with biochemically unclassified leukoencephalopathy. 'Targeted resequencing' of a custom panel including genes coding for mitochondrial proteins was performed in patients with complex III deficiency without a molecular genetic diagnosis. Based on brain magnetic resonance imaging findings in these patients, we selected additional patients from a database of unclassified leukoencephalopathies who were scanned for mutations in *LYRM7* by Sanger sequencing. Targeted sequencing revealed homozygous mutations in *LYRM7*, encoding mitochondrial LYR motif-containing protein 7, in four patients from three unrelated families who had a leukoencephalopathy and complex III deficiency. Two subjects harboured previously unreported variants predicted to be damaging, while two siblings carried an already reported pathogenic homozygous missense change. Sanger sequencing performed in the second cohort of patients revealed *LYRM7* mutations in three additional patients, who were selected on the basis of the magnetic resonance imaging pattern. All patients had a consistent magnetic resonance imaging pattern of progressive signal abnormalities with multifocal small cavitations in the periventricular and deep cerebral white matter. Early motor development was delayed in half of the patients. All patients but one presented with subacute neurological deterioration in infancy or childhood, preceded by a febrile infection, and most patients had repeated episodes of subacute encephalopathy with motor regression, irritability and stupor or coma resulting in major handicap or death. LYRM7 protein was strongly reduced in available samples from patients; decreased complex III holocomplex was observed in fibroblasts from a patient carrying a splice site variant; functional studies in yeast confirmed the pathogenicity of two novel mutations. Mutations in *LYRM7* were previously found in a single patient with a severe form of infantile onset encephalopathy. We provide new molecular, clinical, and neuroimaging data allowing us to characterize more accurately the molecular spectrum of *LYRM7* mutations highlighting that a distinct and recognizable magnetic resonance imaging pattern is related to mutations in this gene. Inter- and intrafamilial variability exists and we observed one patient who was asymptomatic by the age of 6 years.

Received August 1, 2015. Revised November 2, 2015. Accepted November 18, 2015. Advance Access publication January 29, 2016

1 Department of Life Sciences, University of Parma, Parma, Italy
2 Department of Child Neurology, VU University Medical Center, Amsterdam, The Netherlands
3 Unit of Neuromuscular and Neurodegenerative Disorders, Laboratory of Molecular Medicine, 'Bambino Gesù' Children's Hospital, IRCCS, Rome, Italy
4 Unit of Molecular Neurogenetics, Foundation IRCCS Neurological Institute C. Besta, Milan, Italy
5 Molecular Genetics and Genomics Unit, Division of Genetics and Rare Diseases, 'Bambino Gesù' Children's Hospital, IRCCS, Rome, Italy
6 BGI-Shenzhen, Shenzhen 518083, China
7 Shenzhen Key Laboratory of Neurogenomics, BGI-Shenzhen, Shenzhen 518083, China
8 Division of Metabolism, 'Bambino Gesù' Children's Hospital, Rome, Italy
9 Department of Neurology, Children's National Medical Center, Washington, USA
10 Department of Pediatric Neurology, Birmingham Children's Hospital, Birmingham, UK
11 Department of Neurology, Great Ormond Street Hospital, London, UK
12 Developmental Neurosciences, UCL-Institute of Child Health, London, UK
13 Department of Genetic Medicine, Sir Ganga Ram Hospital, New Delhi, India
14 Paediatric Neurology Department, Hospital Dona Estefânia, Centro Hospitalar de Lisboa Central, Lisbon, Portugal
15 Paediatric Department, Unidade Local de Saúde do Baixo Alentejo, Beja, Portugal
16 Child Neuropsychiatry Unit, Spedali Civili, Brescia, Italy
17 Child Neurology Unit, Foundation IRCCS Neurological Institute C. Besta, Milan, Italy

Correspondence to: Enrico Bertini,
Unit for Neuromuscular and Neurodegenerative Disorders,
Laboratory of Molecular Medicine,
Bambino Gesù Children's Hospital, IRCCS,
Viale di San Paolo,
15 - 00146 Rome, Italy
E-mail: enricosilvio.bertini@opbg.net

Correspondence may also be addressed to: Marjo van der Knaap, Department of Child Neurology, Neuroscience Campus Amsterdam, VU University Medical Center, De Boelelaan 1117, 1081 HV Amsterdam, The Netherlands.
E-mail: ms.vanderknaap@vumc.nl

Daniele Ghezzi, Unit of Molecular Neurogenetics, The 'Carlo Besta' Neurological Institute Foundation – IRCCS, via Temolo 4, Milan 20126, Italy. E-mail: dghezzi@istituto-besta.it

Keywords: mitochondria; complex III; leukoencephalopathy; cavitations; *LYRM7*

Introduction

Considering the increasing number of mitochondrial disease genes and the extreme clinical heterogeneity, the strategy to reach a conclusive diagnosis is a complex task for many mitochondrial disorders. There is general awareness that a combination of clinical observations, biochemical evaluation, brain imaging, and muscle biopsies for morphological and functional studies is essential not only to establish a candidate gene approach, but even more in the validation process of causative mutations amongst numerous variants called by next generation sequencing (Wortmann *et al.*, 2015).

Complex III or ubiquinol:cytochrome c oxidoreductase (E.C. 1.10.2.2; cytochrome bc1 complex) is the central component of the respiratory electron transport chain embedded in the inner membrane of mitochondria in eukaryotes. Mammalian complex III possesses a dimeric structure in which each 'monomer' is composed of 11 different subunits (Schägger *et al.*, 1986; Iwata *et al.*, 1998), three of which constitute the catalytic core: MT-CYB (cytochrome b, the only mitochondrial DNA-encoded subunit), CYC1 (cytochrome c1) and UQCRFS1 (Rieske Fe–S protein) (Elstner *et al.*, 2008). The complex III assembly involves a multi-step process and the formation of different assembly intermediates (Graham *et al.*, 1994; Smith *et al.*, 2012). The assembly of the complex is completed when UQCRFS1/Rip1 is inserted in the last step, followed by Qcr10 (Smith *et al.*, 2012).

Deficiencies in complex III are considered to be relatively rare, but perhaps conditions with isolated complex III defect are only less frequently diagnosed because their detection may be more difficult due to the lack of histological and biochemical hallmarks in skeletal muscle biopsies, e.g. no COX-negative or ragged red fibres (Fernández-Vizarra and Zeviani, 2015). Complex III deficiencies have most commonly been associated with mutations in the mitochondrial DNA gene encoding cytochrome b. Mutations in nuclear genes encoding structural complex III subunits have been described in the genes coding for subunit 7 (*UQCRB*, *QCR7* in yeast) (Haut *et al.*, 2003), subunit 6 (*UQCRQ*, *QCR8* in yeast) (Barel *et al.*, 2008), Core 2 (*UQCRC2*, *QCR2* in yeast) (Miyake *et al.*, 2013) and cytochrome c1

(*CYC1*, *CYT1* in yeast) (Gaignard *et al.*, 2013). Mutations in genes encoding two human complex III assembly factors, BCS1L (*BCS1* in yeast) and TTC19 (no yeast orthologue), have been reported in infants with variable clinical presentation and severity (de Lonlay *et al.*, 2001; De Meirleir *et al.*, 2003; Ghezzi *et al.*, 2011; Nogueira *et al.*, 2013). The molecular defect in most complex III-deficient individuals remains to be identified, suggesting that additional assembly factors with deleterious mutations remain to be discovered.

Recently one paper reported a mutation in *LYRM7* (Mzm1 in yeast) (Invernizzi *et al.*, 2013), a homozygous substitution (c.73G>A), predicting a drastic change in a highly conserved amino acid residue (p.D25N) (Invernizzi *et al.*, 2013); the *mzm1* deleted yeast strain expressing the $mzm1^{D25N}$ mutant allele showed temperature-sensitive respiratory growth defect, decreased oxygen consumption, impaired maturation/stabilization of the UQCRFS1/Riske Fe-S protein, and reduced complex III activity and amount (Invernizzi *et al.*, 2013).

Since its introduction into medicine, MRI has emerged as a valuable tool for the differential diagnosis of leukoencephalopathies, including mitochondrial encephalomyopathies (Van der Knaap and Valk, 2005). Several examples of how MRI pattern recognition was central in the identification of novel disorders and mitochondrial defects include leukoencephalopathy with brainstem and spinal cord involvement with elevated lactate (LBSL) caused by mutations in *DARS2* encoding mitochondrial aspartyl-tRNA synthetase, (Scheper *et al.*, 2007); leukoencephalopathy with thalamus and brainstem involvement with elevated lactate (LTBBL) caused by mutations in *EARS2*, the gene encoding mitochondrial glutamyl-tRNA synthetase (Steenweg *et al.*, 2012); the leukoencephalopathy caused by mutations in *NUBPL*, encoding an iron-sulphur cluster assembly factor for complex I (Kevelam *et al.*, 2013); and the leukoencephalopathy caused by mutations in *APOPT1*, encoding a mitochondrial protein that seems to connect apoptosis with increased reactive oxygen species production (Melchionda *et al.*, 2014). In most mitochondrial leukoencephalopathies, white matter and, to a lesser degree, grey matter structures are affected with a peculiar distribution that has enabled recognition of specific genetic forms with or even without the integration of a specific defect in the mitochondrial respiratory chain enzymes (Scheper *et al.*, 2007; Steenweg *et al.*, 2012).

In the present study we describe five novel mutations in *LYRM7* found in five unrelated subjects, and an already described *LYRM7* mutation (Invernizzi *et al.* 2013) in two siblings. All patients were characterized by a similar and distinct MRI pattern of a progressive leukoencephalopathy with numerous small cavitations in the periventricular and deep cerebral white matter; most of them showed a severe complex III defect.

Materials and methods

Standard protocol approvals, registrations, and patient consent

The study was approved by the Ethical Committees of the Children Hospital Bambino Gesù, Rome, Italy, the Neurological Institute Besta, Milan, Italy, and the VU University Medical Center, Amsterdam, The Netherlands, in agreement with the Declaration of Helsinki. Informed consent was signed by the parents of the patients.

Patients

Patients 1, 2, 3 and 4 were included in a targeted resequencing study performed in 23 patients displaying biochemical defects in mitochondrial respiratory chain complex III. Based on the MRI documented in Patient 1, we selected from the Amsterdam and Washington databases, which together contain more than 4000 cases with an unclassified leukoencephalopathy, three additional patients (Patients 5, 6 and 7) with a typical neuroimaging pattern, together with two additional patients that were considered to have an atypical distribution of lesions. The MRIs of all patients were systematically analysed as previously described (van der Knaap *et al.*, 1999) and clinical histories and laboratory findings were reviewed.

Molecular studies

Genomic DNA was extracted by standard methods from leucocytes. For Patient 1, targeted resequencing was performed at the BGI-Shenzhen (BGI-Shenzhen, Shenzhen, China). A custom probe library was used for targeted resequencing (Agilent SureSelectXT Custom Kit) designed to capture coding exons and flanking intronic stretches (20 nt) of 1381 genes known to be functionally related to mitochondrial disorders ('Mitoexome', Calvo *et al.*, 2012), followed by deep sequencing using Illumina HiSeq technology, providing 255× effective mean depth. For Patients 2 and 4, a customized gene panel (TruSeq Custom Amplicon, Illumina) containing 72 genes previously associated with mitochondrial disorders and isolated mitochondrial respiratory chain complex deficiency ('Mitoiso' panel; details available upon request) was used for library preparation; then samples were analysed by a MiSeq system (Illumina), with 100× effective mean depth. Sanger sequencing was used to validate the parallel sequencing data, as well as to check variant segregation in families.

To assess the functional effect of splice-site variants, polyA+RNA was purified from cultured skin fibroblasts and reverse-transcribed to cDNA using the First Strand cDNA Synthesis kit (Roche Diagnostics).

Functional studies

Human samples

Protein studies: For structural studies fibroblasts were processed as described elsewhere (Nijtmans *et al.*, 2002). Briefly, mitochondrial membranes were isolated from 2.6×10^6 cells.

Pellets were suspended in phosphate-buffered saline and solubilized for 10 min with digitonin (2 mg/mg protein), followed by 1% (v/v) lauryl maltoside (Sigma Aldrich). Proteins (35–80 µg) were separated by first dimensional blue native gel electrophoresis (BNGE) in a linear 5–13% gradient non-denaturing gel; thereafter, proteins were transferred to a polyvinylidene difluoride (PVDF) membrane and subjected to western blotting. For electrophoresis in sodium dodecyl sulphate polyacrylamide gels (SDS-PAGE), 30 µg of fibroblast mitochondria were loaded in a 12% denaturing gel. For immunoblot analysis, PVDF membranes were probed with monoclonal antibodies and reactive bands were detected using LiteAblot® Extend Long Lasting Chemiluminescent Substrate (Euroclone). Densitometry analysis was performed using Quantity One software (Bio-Rad).

Antibodies: Complex I – 39 kDa subunit (NDUFA9); complex II – 70 kDa (SDHA); complex III – UQCRC1 (Core protein 1), – UQCRC2 (Core protein 2) and – UQCRFS1 (Rieske Fe–S protein) subunits; complex IV – subunit II (COXII); complex V – subunit alpha (ATP5A1), and porin (VDAC) were purchased from MitoSciences (Eugene). LYRM7 antibody was purchased from Abcam.

Yeast experiments

Strains, media and miscellaneous yeast procedures: Yeast strains were BY4741 (*MATa*; *his3Δ1*; *leu2Δ0*; *met15Δ0*; *ura3Δ0*) and its isogenic *mzm1:KanMX4* null mutant (Euroscarf collection). Strains were grown in synthetic complete (SC) defined medium (6.9 g/l YNB) without amino acids (ForMedium) supplemented with 1 g/l dropout mix without uracil (Baruffini *et al*, 2010). Carbon sources (Carlo Erba Reagents) were added as indicated in the text in liquid phase or after solidification with 20 g/l agar (ForMedium). Transformation of *Saccharomyces cerevisiae* has previously been described (Schiestl and Gietz, 1989).

Construction of yeast mutant alleles and DNA manipulation: Plasmid pFL38 harbouring wild-type *MZM1* allele has been previously described (Invernizzi *et al*, 2013). The pFL38-*MZM1* construct was used as a template to introduce stop codon at positions Q70 or L64 duplication by PCR-based site directed mutagenesis, using the primers listed in Supplementary Table 1. All constructs were verified by Sanger sequencing.

Respiration measurement and respiratory chain complex activities: Oxygen consumption rate was measured at 30°C from yeast cells cultured for 18 h at 28°C in SC medium supplemented with glucose at non-repressing concentration of 0.6% using a Clark-type oxygen electrode (Oxygraph System Hansatech Instruments) with 1 ml of air-saturated respiration buffer (0.1 M phthalate–KOH, pH 5.0), 10 mM glucose. The reaction started by addition of 20 mg of wet-weight cells, as described (Goffrini *et al*, 2009). NADH-cytochrome c oxidoreductase activity (NCCR) and complex IV specific activities were measured spectrophotometrically on a mitochondrial-enriched fraction prepared as previously described (Barrientos *et al*., 2009; Soto *et al*., 2009) after a cellular growth to a concentration of 1.5–2 OD_{600} in SC medium supplemented with 2% galactose and 0.2% glucose.

Mitochondrial protein purification and SDS-PAGE

Mitochondria were purified as previously reported (Goffrini *et al*., 2009). Protein concentration was quantified according to Bradford (Bio-Rad). Mitochondrial proteins (15 µg) were separated by 12% SDS-PAGE, and electro-blotted onto nitrocellulose filters that were then incubated with anti-Rip1 antibodies (a generous gift from Prof. Alexander Tzagoloff) and porin (Abcam Mitoscience). ECL Western Blotting Substrate (Thermo Scientific Pierce) was used for final detection.

Results

Clinical and laboratory findings

The clinical details of the patients in whom we found mutations in *LYRM7* are reported in Supplementary Table 2. A clinical report on Patient 1 is provided here followed by a summary report on the remaining patients to highlight the common clinical features.

Patient 1 is a male born at term from parents that denied consanguinity. Mild developmental delay was noted at 8 months of age because he was not able to sit without support. At age 11 months he was admitted to hospital for psychomotor regression, marked hypotonia and failure to thrive. Neurological examination revealed facial weakness, swallowing difficulties, axial hypotonia with spastic hypertonia of arms and legs, and bilateral pes equinus. Plasma lactate acid was increased to 3.73 mmol/l (normal values: 0.444–2.22 mmol/l), and no organic aciduria was detected. During the hospitalization percutaneous endoscopic gastrostomy became necessary. At follow-up, the clinical course was characterized by multiple episodes of vomiting and metabolic acidosis provoked by infectious illnesses and requiring hospitalization. These episodes led to psychomotor regression. Treatment with intravenous dexamethasone (10 mg/kg/d) resulted in some clinical improvement. Neurological examination at age 3 years showed severe psychomotor delay; language was limited to ~20 words. The child had axial hypotonia, severe spastic-dystonic tetraparesis of the limbs and marked kyphoscoliosis. At age 3 years and 8 months, a sudden deterioration of the clinical picture occurred with prolonged apnoea and cardiocirculatory arrest that required tracheostomy. Cardiac involvement was excluded whereas liver ultrasound displayed increased volume with irregular structure. Transaminases and creatine kinase were always in the normal range. Visual-evoked and brainstem auditory potentials were abnormal. Of note, he presented with recurrent episodes of VII cranial nerve paralysis, improving on dexamethasone treatment. The latest neurological examination at 7.5 years showed severe psychomotor delay, ophthalmoplegia, nystagmus, facial weakness and spastic-dystonic tetraparesis. Muscle and skin biopsy were performed at 18 months. The spectrophotometric determination of mitochondrial respiratory chain complex activities displayed an isolated 75% reduction of complex III normalized to citrate synthase (complex III/CS) in muscle biopsy.

Of the remaining six subjects from five families, two were sibs (Patients 3 and 4). The other four patients (Patients 2,

5, 6 and 7) were sporadic, but two of them (Patients 2 and 7) originated from inbred families. Most patients manifested with a mild delay of motor milestones. Three of six patients presented with an episode of subacute encephalopathy characterized by psychomotor regression, often irritability, and sometimes stupor or coma, within the first 2 years of life. One patient presented with such an episode at the age of 6 years, and one at 14 years, although both patients already displayed developmental delays and mild motor dysfunction. One of the sibling patients is still asymptomatic at age 6 years. These episodes were recurrent in most patients and were accompanied by lactic acidosis. They were typically induced by febrile illnesses, but sometimes without any relevant antecedent. Most patients displayed failure to thrive and recurrent vomiting; many were eventually tube-fed. Following a period of a few years all affected children were severely disabled and one died at 7 years.

The laboratory results of the patients are summarized in Supplementary Table 3. Metabolic studies only revealed increased lactic acid in body fluids. The biochemical analysis of mitochondrial respiratory chain in muscle biopsy, when available, consistently showed a marked defect of complex III.

MRI abnormalities

The details of the MRI findings are provided in Supplementary Table 4. MRIs of Patient 1 are described in detail here, followed by a summary of the MRI findings in the other patients.

In Patient 1 the first MRI [Fig. 1A(a–h)] performed at age 19 months showed extensive, inhomogeneous, partially multifocal and partially confluent signal abnormalities in the periventricular and deep cerebral white matter, relatively sparing the directly subcortical white matter. Fluid-attenuated inversion recovery (FLAIR) images showed numerous isolated cavitations within the abnormal white matter, surrounded by a rim of solid tissue [Fig. 1A(e and f)]. The corpus callosum was abnormal in signal and contained multiple cavitations [Fig. 1A(b and f)]. Signal abnormalities without cavitations were present in the posterior limb of the internal capsule and central tegmental tracts in the brainstem. Signal abnormalities with cavitations were present in the border between medulla oblongata and cervical spinal cord [Fig. 1A(b and h)]. Diffusion restriction with low apparent diffusion coefiicient (ADC) values was observed in the non-cavitated abnormal white matter [Fig. 1A(c and d)]. No enhancement after contrast was present. The second MRI [Fig. 1A(i–p)] performed at age 3.5 years displayed an increase in the extent of the cerebral white matter abnormalities, including the corpus callosum, containing high numbers of small, roundish cysts. The middle cerebellar peduncles and cerebellar white matter were also affected, right more than left, as well as the cervicomedullary junction [Fig. 1A(k and l)]. Again, diffusion restriction with low ADC values was observed in the non-cavitated abnormal white matter [Fig. 1A(o and p)].

The other MRIs confirmed such a pattern (Fig. 1B). The candidate gene approach of selecting the MRI from undiagnosed patients from the Amsterdam and Washington databases designated five patients who showed an MRI pattern of cavitating leukodystrophy, although only three patients with bialellic mutations in *LYRM7* were the ones considered to have a typical distribution of lesions. In the other two patients the cystic cerebral white matter lesions remained more limited in extent without signal abnormalities outside the cysts (one patient) or largely confined to the parieto-occipital region (the other patient). This result confirmed the rarity of *LYRM7*-related cavitating leukodystrophy in a large cohort of patients with unclassified leukodystrophies and the diagnostic value of MRI for this genetic disorder. Early MRIs in the patients with *LYRM7* mutations showed limited, multifocal or more confluent signal abnormalities involving the periventricular and deep cerebral white matter, already containing small cysts in the earliest stages [Fig. 1B(a and b)]. Over time the abnormalities became more extensive [Fig. 1B(c–f)]. The corpus callosum was often, but not invariably involved in the process. The middle cerebellar peduncles, high cervical spinal cord and the cervicomedullary junction were frequently affected [Fig. 1B(g and h)]. In one patient, cystic degeneration of the cervical spinal cord occurred. Diffusion restriction was typically present, either diffuse or multifocal, often especially in the rim of cysts. Contrast enhancement was variable, if present typically in the rim of cysts [Fig. 1B(i–l)]. Interestingly the MRI pattern of the asymptomatic Patient 4 showed similar typical abnormalities [Fig. 1B(a and b)].

Targeted resequencing and Sanger validation

The details of the mutations identified are provided in Supplementary Table 3. Parallel targeted resequencing of the Mitoexome (Calvo *et al.*, 2012) on Patient 1 and of the Mitoiso gene panel on Patients 2 and 4 were performed, respectively. After excluding previously annotated single nucleotide changes occurring with high frequency in populations (frequency $>0.1\%$), we prioritized the retained changes identified in each gene according to the presence of homozygous or compound heterozygous variants with functional impact (i.e. non-synonymous variants and changes affecting splice sites), as expected for a recessive inherited trait. In Patient 1, this filtering led to the identification of a single gene entry, *LYRM7* (NC_000005.10, NM_181705.3), in which a homozygous mutation was recognized (c.244 + 5insG) (Fig. 2A and B). Polyemrase chain reaction (PCR) and sequencing analysis of cDNA obtained from Patient 1 revealed skipping of exon 4 (Fig. 2C and D) resulting in a frameshift and predicting the synthesis of a truncated protein (p.K82Nfs*10), confirming the deleterious effect of the intronic variant c.244 + 5insG on the splicing process of *LYRM7* transcript.

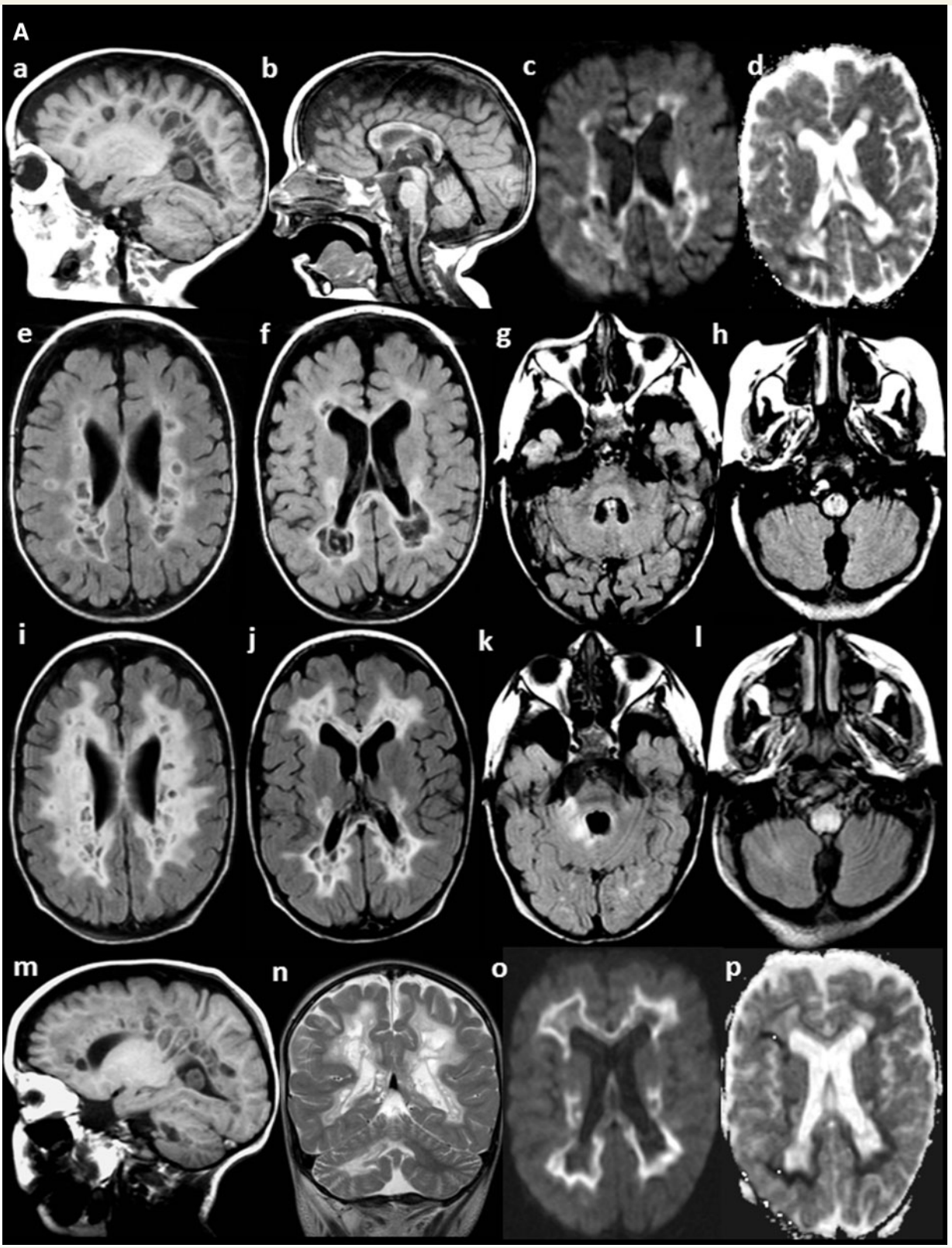

Figure 1 Brain MRI. (**A**) MRI of Patient 1 at the ages 19 months (**a–h**) and 3.5 years (**i–p**). At 19 months, the sagittal T_1-weighted (**a** and **b**) and axial FLAIR (**e** and **f**) images show signal abnormality and multiple small cysts in the periventricular and deep cerebral white matter, also involving the corpus callosum (**b**) and cervicomedullary junction (**b** and **h**). The diffusion-weighted images (**c**) suggest diffusion restriction in the abnormal, non-cystic white matter, cofirmed by low signal on the ADC map (**d**). At 31 months, the white matter abnormalities have increased in extent and the cysts have in part become smaller (**i**, **j** and **m**). The middle cerebellar peduncle and cerebellar white matter are affected on the right (**k** and **n**). The cervicomedullary junction is still abnormal (**l**). Diffusion restiction is present in the solid part of the abnormal white matter (**o** and **p**).

(continued)

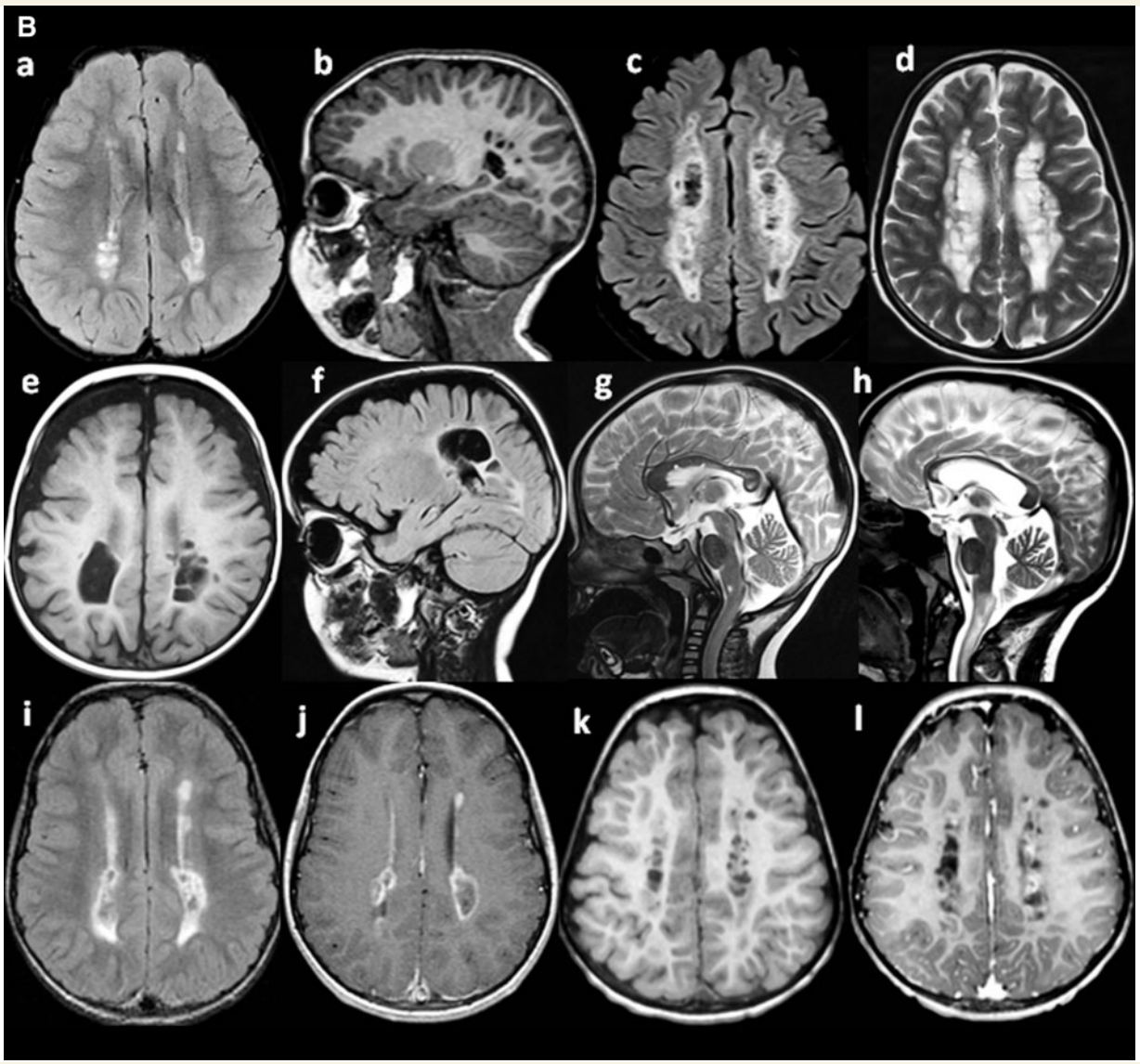

Figure 1 Continued. (**B**) Illustration of extra MRI features in Patients 4 (**a** and **b**), 6 (**c** and **d**), 7 (**e** and **f**), 2 (**g**), 6 (**h**), 5 (**i** and **j**) and 3 (**k** and **l**). At the age of 2.5 years, the MRI of Patient 4, clinically asymptomatic, shows starting multifocal abnormalities in the periventricularwhite matter with small cysts (**a** and **b**). At age 14 years, the MRI of Patient 6 shows extensive signal abnormalities in the periventricular and deep cerebral white matter with numerous small cysts (**c** and **d**). The cysts in Patient 7 are larger (age 3 years; **e** and **f**). In Patient 2, a small lesion is seen at the cervicomedullary junction (1.8 years; **g**), while a much larger lesion is seen extending into the cervicospinal cord in Patient 6 (age 14; **h**). In Patient 5, enhancement of the rim of the sesions is seen (10 years; **i** and **j**), whereas small multifocal enhancing spots are seen in Patient 3 (6 years; **k** and **l**).

Similarly, a single homozygous variant in *LYRM7* remained after the filtering procedure in Patients 2 and 4: a trinucleotide duplication c.193_195dup (p.L66dup) was identified in the former (Fig. 2E), and the previously described c.73G>A missense change (p.D25N) in the latter (Fig. 2F). Sanger sequencing confirmed the presence of mutations in both patients (Fig. 2E and F), and cosegregation with the disorder; moreover the c.73G>A change was homozygous in Patient 3, who was the brother of Patient 4, and heterozygous in their parents (Fig. 2G).

Sanger sequencing of the entire coding sequence of *LYRM7* and intron-exon boundaries was performed in three additional patients. Patient 5 was found homozygous for the c.243_244+2del, which is predicted to dramatically affect recognition of the splice donor motif of exon 4 and likely impair proper RNA splicing (Fig. 2H and I), while Patients 6 and 7 were found to be homozygous for the c.214C>T (p.Q72*) (Fig. 2L), and c.37delA (p.T13Hfs*17) (Fig. 2M) mutations, respectively.

Functional studies

Human

Biochemical findings on spectrophotometric analysis of mitochondrial respiratory chain enzymes in muscle biopsy of Patients 1–5 are summarized in Supplementary Table 3,

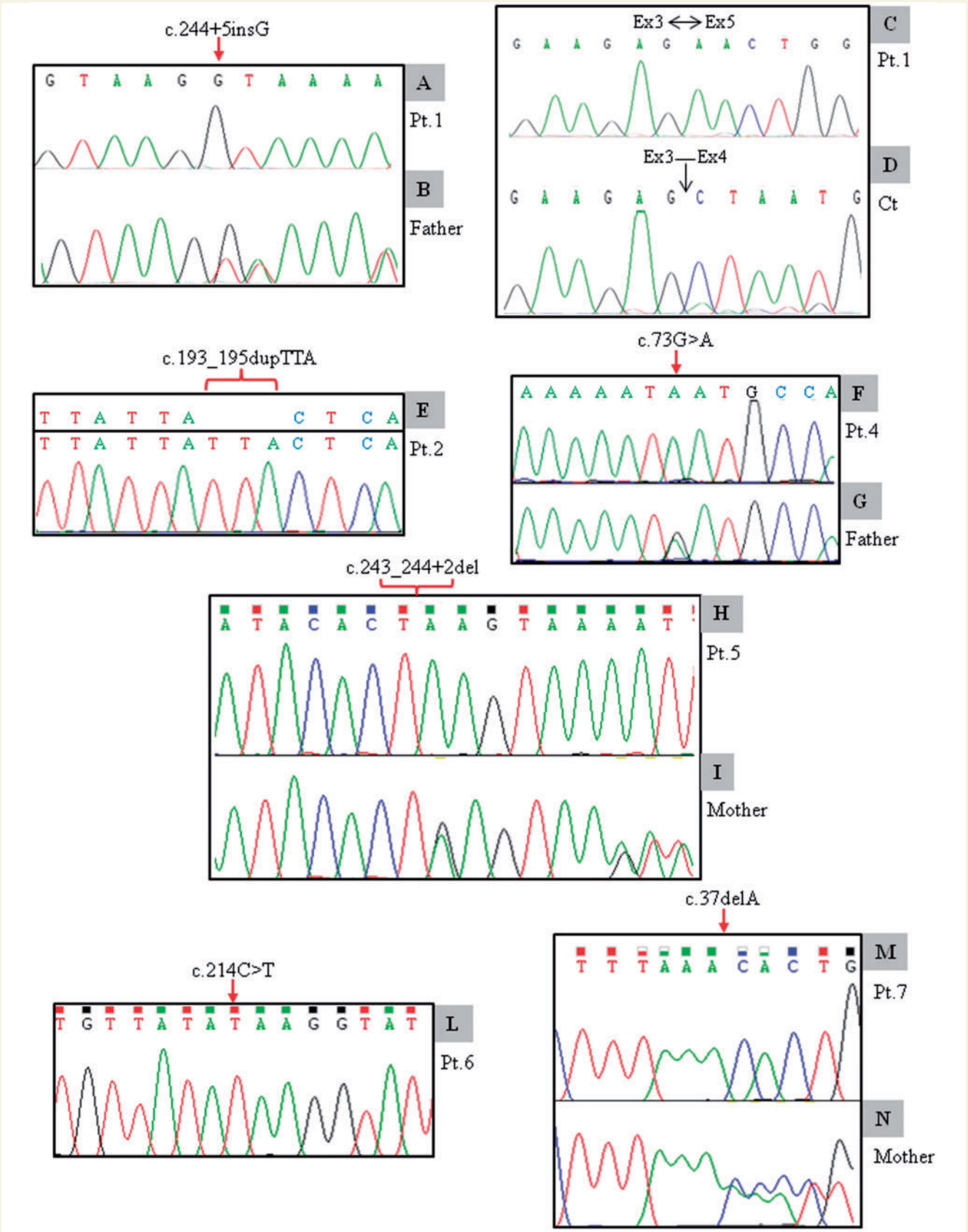

Figure 2 Genetic features. Electropherograms of the genomic region encompassing the mutation c.244 + 5insG, homozygous in Patient 1 (**A,** Pt.1) and heterozygous in both parents (**B**). The mutation produces a skipping of exon 4 in the *LYRM7* transcript of Patient 1 (**C** and **D**). Sequencing analysis displayed in Patient 2 (Pt.2) a TTA c.193_195 duplication (**E**), and in Patient 4 (Pt.4) a homozygous c.73G > A change (**F**); the latter was heterozygous in the parents (**G**). Patient 5 (Pt.5) was homozygous for a 4-bp deletion, the c.243_244 + 2del (**H**), heterozygous in both parents (**I**). Patient 6 (Pt.6) was homozygous for the missense mutation c.214C > T [p.Q72*] (**L**). Patient 7 (Pt.7) was homozygous for the c.37delA (**M**), heterozygous in both parents (**N**).

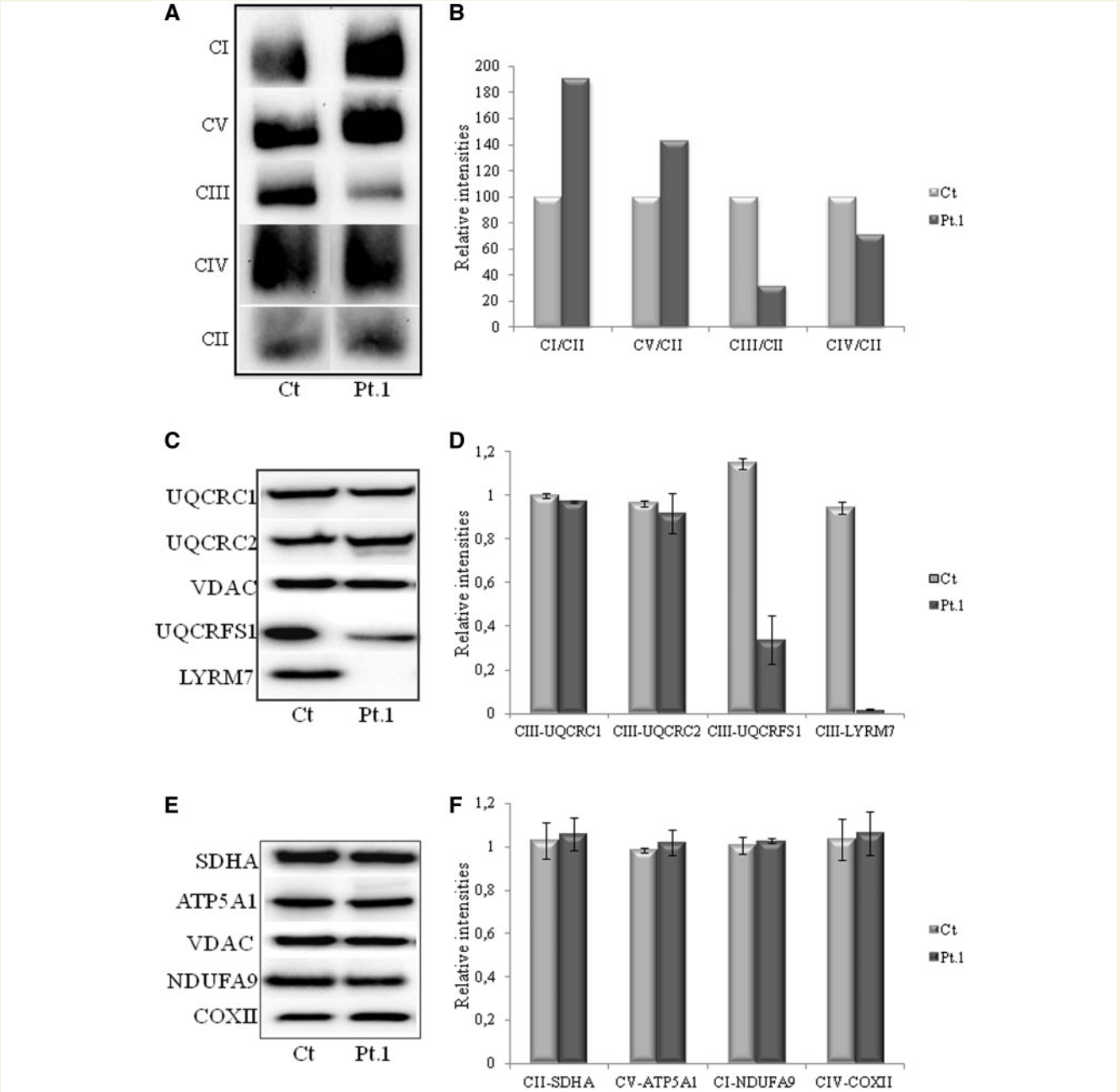

Figure 3 Western blotting analysis on blue native and SDS gel electrophoresis. (**A**) One-dimensional BNGE performed on fibroblast mitochondria of control (Ct) and Patient 1 (Pt.1) was subjected to western blotting. Antibodies against the UQCRC2 subunit revealed a severe reduction of complex III (CIII), whereas an increased amount of complex I (CI) and V (CV) was evident using antibodies against NDUFA9 and ATPase α (ATP5A1) subunits, respectively. The signal of complex II (CII) SDHA subunit was used as a control for equal loading and for normalization in the densitometry analysis. The relative intensities are reported in **B**. The same samples were separated by denaturing SDS-PAGE; specific antibodies against complex III (UQCRC1, UQCRC2, UQCRFS1, and LYRM7), reported in **C**, and specific antibodies against complex II (SDHA), complex V (ATP5A1), complex I (NDUFA9), and complex IV (COXII), reported in **E**, were used for immunodetection. The mitochondrial protein porin (VDAC) was used as a control for equal loading and for normalization in the densitometry analysis. The relative intensities are reported in **D** and **F**, respectively. The quantity of LYRM7 was found to be severely affected, as well the UQCRFS1 subunit.

and show reduction of complex III activity. In Patient 6 a muscle sample was not available; in Patient 7 the enzyme activity of complex III was initially not measured and by the time biallelic mutations in *LYRM7* were found, no residual muscle sample was available for western blotting and spectrophotometric analysis. In samples from Patient 1's fibroblasts, BNGE displayed a severe reduction of the entire complex III complex associated to a compensatory increase of complex I (Fig. 3A and B). SDS-denaturing gel displayed a dramatic reduction of LYRM7, as expected for the frameshift predicted by cDNA analysis, associated with a partial reduction of UQCRFS1 (Fig. 3C and D). Two

additional subunits of complex III (UQCRC1 and UQCRC2) were normally expressed, as well as subunits that are part of other mitochondrial respiratory chain complexes (Fig. 3E and F). A strong decrease of LYRM7 amount was observed also in fibroblasts from Patient 2 and in skeletal muscle from Patients 3 and 4 (Supplementary Fig. 1), despite the latter subjects carrying a missense mutation whereas Patient 2 harboured a trinucleotide duplication causing the introduction of an extra amino acid in the protein.

Yeast

To validate the pathogenicity of the mutations p.Q72* (found in Patient 6) and p.L66dup (found in Patient 2) we used the yeast *S. cerevisiae* as a model system taking advantage of the presence of the orthologous gene *MZM1*. We first introduced the changes equivalent to the human mutations into the yeast *MZM1* wild-type gene cloned in a centromeric monocopy vector. The human Q72* and L66dup mutations correspond to yeast Q70* and L64dup, respectively. The *MZM1*, *mzm1*^{Q70*} and *mzm1* ^{L64dup} constructs were used to transform the *mzm1*Δ null mutant, giving rise to *mzm1*Δ/*MZM1*, *mzm1*Δ/*mzm1*^{Q70*} and *mzm1*Δ/*mzm1* ^{L64dup} yeast strains. The *mzm1*Δ strain was transformed also with the empty vector as a negative control.

To detect a possible respiratory growth defect, equal amounts of serial dilutions of cells from exponentially grown cultures were spotted onto SC plates supplemented with either 2% glucose or 2% ethanol. The growth was scored after 3 days of incubation at 28°C or 37°C. A clear growth defect of the *mzm1*Δ/*mzm1*^{Q70X} and *mzm1*Δ/*mzm1* ^{L64dup} was observed in ethanol-containing plates incubated at 28°C and a complete growth inhibition at 37°C (Fig. 4A), similar to the *mzm1*Δ mutant (Atkinson *et al.*, 2010; Invernizzi *et al.*, 2013).

To better define the oxidative growth deficiency, we measured oxygen consumption, NCCR and COX activity and cytochromes spectra. The O_2 consumption rates of *mzm1*Δ/*mzm1*^{Q70*}and *mzm1*Δ/*mzm1*^{L64dup} were ~60% less than that of *mzm1*Δ/*MZM1* and similar to that displayed by *mzm1*Δ (Fig. 4B). In both mutant strains as well as in the null strain *mzm1*Δ biochemical assays showed a severe and specific decrease of complex III activity (40-50% residual activity) whereas complex IV (cIV, cytochrome *c* oxidase, COX) activity was normal (Fig. 4C). In addition both mutants, *mzm1*Δ/*mzm1*^{Q70*} *mzm1*Δ/*mzm1*^{L64dup} exhibited a significant reduction of the peak at 560 nm, corresponding to respiratory cyt *b* (not shown). These results are consistent with the respiratory growth defect observed in the mutant strains *mzm1*Δ/*mzm1*^{Q70*} and *mzm1*Δ/*mzm1*^{L64dup} and paralleled the reduction of respiratory activity.

Cells lacking Mzm1 have impaired complex III activity due to attenuated levels of the Rieske iron–sulphur protein, (Rip1p in yeast) insertion. To evaluate the effects of the *mzm1*^{Q70X} and *mzm1*^{L64dup} mutations on Rip1p biogenesis and complex III function, we studied mitochondria purified from *mzm1*Δ/*MZM1*, *mzm1*Δ/*mzm1*^{Q70*} *mzm1*Δ/*mzm1*^{L64dup} and *mzm1*Δ strains, cultured at 28°C in SC medium. Mitochondrial proteins were resolved by SDS-PAGE and immune-visualized by western blot analysis. As shown in Fig. 4D, the Rip1 level was greatly reduced in *mzm1*^{Q70*} and *mzm1*^{L64dup} mutants that behaved as the null mutant *mzm1*Δ (Cui *et al.*, 2012). These data support the pathogenic role of their human counterpart.

Discussion

MRI is a sensitive tool to diagnose leukoencephalopathies. It is also of great help in distinguishing different individual disorders within the large group of all leukoencephalopathies by distinct patterns of abnormalities. In recent years it has been shown multiple times that this MRI-based approach also works very well for mitochondrial leukoencephalopathies. Consistent and striking patterns of abnormalities could be linked to specific mitochondrial dysfunctions and gene defects, facilitating the differential diagnosis of mitochondrial leukoencephalopathies and allowing molecular screening to be limited to a subset of genetic defects, either known or unknown, that affect different functions of mitochondria. The often striking MRI patterns may even allow the identification of the causative genes using the brain imaging and omitting the biochemical data (Morato *et al.*, 2014).

In 2013, a homozygous mutation in *LYRM7* was described by candidate gene approach in a single individual to be associated with early onset, fatal severe encephalopathy, lactic acidosis and profound, isolated complex III deficiency in skeletal muscle (Invernizzi *et al.*, 2013). The brain MRI of this patient showed a leukoencephalopathy. However, the pattern of distribution and progression of the white matter lesions associated with *LYRM7* mutations were not outlined. In the present study, we extended that initial observation by providing evidence that *LYRM7* mutations recur in cases with leukoencephalopathy associated with a biochemical defect of mitochondrial respiratory chain complex III, and reporting a more complete assessment of the phenotypic variation associated with these molecular lesions.

By targeted resequencing on a cohort of patients with mitochondrial respiratory chain complex III deficiency, we were able to identify homozygosity for *LYRM7* mutations in three unrelated families. Three additional patients were selected for mutation analysis in the same gene on the basis of the distinctive brain MRI, indicating that the radiological phenotype associated with mutations in *LYRM7* is distinctive. On the other hand, our failure in identifying *LYRM7* mutations in complex III-deficient patients with different MRI patterns suggests that the MRI phenotype associated with *LYRM7* mutations is relatively homogeneous. The characteristic MRI profile consists of essentially multifocal white matter abnormalities in the periventricular and deep cerebral white matter, coalescing to more confluent abnormalities. The focal lesions were rarefied and

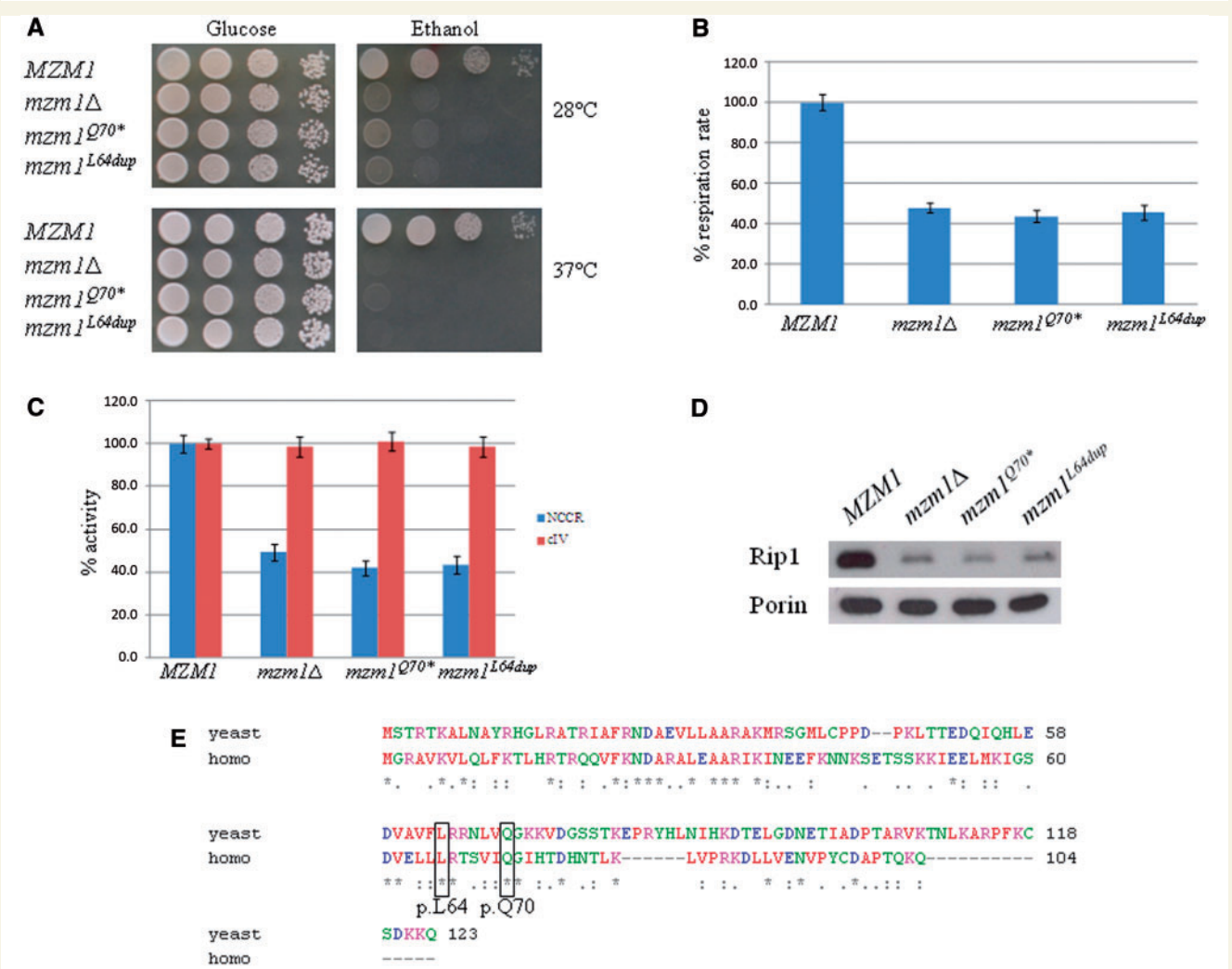

Figure 4 Phenotypes of the yeast model. (**A**) Oxidative growth. *mzm1*Δ strains harbouring *MZM1* wild-type allele, the *mzm1*^{Q70*} or the *mzm1*^{L64dup} allele or the empty vector were serially diluted and spotted on SC agar plates supplemented with 2% glucose or 2% ethanol. Plates were incubated at 28°C or 37°C. (**B**) Oxygen consumption rates were recorded on cells grown at 28°C in SC medium supplemented with 0.6% glucose. Respiratory rates were normalized to the wild-type strain for which the respiratory rate was 30.0 nmol O_2/min/mg. Values are the mean of at least three independent experiments. (**C**) NADH-cytochrome c oxidoreductase (NCCR) and complex IV (cIV) specific activities were recorded on a mitochondrial-enriched fraction from cells grown at 28°C in SC medium supplemented with 2% galactose and 0.2% glucose. Values were normalized to that of *MZM1* parental strain and represented as mean of at least two independent experiments. (**D**) Immunoblot analysis: 15 μg of mitochondrial proteins were resolved with 12% SDS-PAGE, blotted on nitrocellulose membranes and the Rip1 protein was immunovisualized by a specific antibody. The mitochondrial protein Porin was used as equal loading control. (**E**) Protein sequence alignment (ClustalW) of the yeast Mzm1 and human LYRM7. The black rectangles indicate the conserved amino acids mutated in patients and modelled in yeast.

cystic, resulting in a peculiar row of small cystic lesions around the ventricles. The corpus callosum was variably affected. The cerebral cortex and central grey matter nuclei were consistently spared. Frequently diffusion restriction was seen in the abnormal white matter, especially in the rims of the small cystic lesions. Proton magnetic resonance spectroscopy was performed in three patients and showed elevated lactate in two. Within the posterior fossa, mainly the middle cerebellar peduncles could be involved. Cervical spinal cord signal abnormalities were seen in most patients. Follow-up MRIs were available for two patients (Patients 1 and 5) and showed an increase in extent of the cerebral and spinal cord abnormalities. Among the analysed subjects with complex III deficiency and without *LYRM7* mutations, none had the same clinical and radiological presentation as the *LYRM7*-positive patients and the few individuals with leukoencephalopathy showed only slight white matter changes without cavitations. Interestingly it should be noted that such typical MRI abnormalities were identified in an asymptomatic 6-year-old girl whose elder sibling showed early onset manifestations of delayed motor milestones and psychomotor regression at age 6 years following a febrile illness, which emphasizes the occurrence of clinical heterogeneity.

Functional studies in human samples (Patients 1–4) and yeast mutagenesis experiments (for mutations found in Patients 2 and 6) confirmed mutations pathogenicity and their link with impaired complex III. All the identified *LYRM7* mutations, irrespective of their type (nonsense, missense, frameshift, and splice-site) were associated with a strong decrease in protein level. Measurement of mitochondrial respiratory chain activities in available muscle biopsies displayed a specific complex III defect. Immunoblot analyses showed reduced amount of the holocomplex and supported the hypothesized role of LYRM7 on the last step of the complex III assembly; in fact, despite the normal amount of UQCRC1 and UQCRC2, which are components of the pre-complex III_2 intermediate, a dramatic reduction was evident for UQCRFS1, which is part of the mature complex III. In yeast cells expressing $mzm1^{Q70*}$ or $mzm1^{L64dup}$ mutant alleles, the oxidative growth, the oxygen consumption rate, NCCR-specific activity and Rip1 amount were markedly reduced and were comparable to values obtained in the *mzm1*Δ null mutant. These results indicate that both yeast alleles expressing p.Q70* and p.L64dup changes behave as null alleles, suggesting the pathogenicity of the corresponding human Q72* and L66dup mutations.

Mzm1 in yeast, and possibly LYRM7 in humans (Sánchez *et al*. 2013), plays a role in the last steps of complex III assembly, being involved in the maturation of UQCRFS1/Rip1, an essential catalytic subunit of complex III (Atkinson *et al*., 2011; Cui *et al*., 2012). Overexpression of epitope-tagged human LYRM7 resulted in elevated UQCRFS1 in the mitochondrial soluble fraction and impaired the assembly of mature complex III, while down-regulation of *LYRM7* caused a decrease in the amount of UQCRFS1 (Fernández-Vizarra and Zeviani, 2015); moreover, co-immunoprecipitation assays revealed that LYRM7 and UQCRFS1 interacted in a low molecular mass intermediate (Sánchez *et al*. 2013). Thus, the proposed function of LYRM7 was to bind and stabilize UQCRFS1 in the mitochondrial matrix prior to the incorporation of UQCRFS1 into complex III in the inner mitochondrial membrane by BCS1L.

Differently from what is known for *BCS1L* and *TTC19*, whose causative mutations have recurrently been reported (Ardissone *et al*., 2015; Koch *et al*., 2015; Fernández-Vizarra and Zeviani, 2015), only one mutation has previously been described in *LYRM7* (Invernizzi *et al*., 2013), suggesting a minor impact of dysregulated function of this protein in human disease. By reporting five novel unrelated cases with biallelic *LYRM7* mutations, we document a more important contribution of LYRM7 lesions as a cause of complex III deficiency. Our findings confirm previous observations indicating the requirement of LYRM7 for proper complex III assembly, possibly functioning as a soluble mitochondrial matrix chaperone for UQCRFS1, the last catalytic subunit to be incorporated into the holocomplex (Sánchez *et al*., 2013).

Funding

This work received financial support from the Telethon Grant GUP09004 and GGP11011, the Italian Ministry of Health (GR2010–2316392), the Pierfranco and Luisa Mariani Foundation and the Italian Association of Mitochondrial Disease Patients and Families (Mitocon). A grant from Shenzhen Municipal of Government of China (CXB201108250094A) is also acknowledged.

Supplementary material

Supplementary material is available at *Brain* online.

References

Ardissone A, Granata T, Legati A, Diodato D, Melchionda L, Lamantea E, et al. Mitochondrial complex III deficiency caused by TTC19 defects: Report of a Novel Mutation and Review of Literature. JIMD Rep 2015; 22: 115–20.

Atkinson A, Khalimonchuk O, Smith P, Sabic H, Eide D, Winge DR. Mzm1 influences a labile pool of mitochondrial zinc important for respiratory function. J Biol Chem 2010; 285: 19450–9.

Atkinson A, Smith P, Fox JL, Cui TZ, Khalimonchuk O, Winge DR. The LYR protein Mzm1 functions in the insertion of the Rieske Fe/S protein in yeast mitochondria. Mol Cell Biol 2011; 31: 3988–96.

Barel O, Shorer Z, Flusser H, Ofir R, Narkis G, Finer G, et al. Mitochondrial complex III deficiency associated with a homozygous mutation in UQCRQ. Am J Hum Genet 2008; 82: 1211–16.

Barrientos A, Fontanesi F, Díaz F. Evaluation of the mitochondrial respiratory chain and oxidative phosphorylation system using polarography and spectrophotometric enzyme assays. Curr Protoc Hum Genet 2009; 19: Unit19.3.

Baruffini E, Ferrero I, Foury F. In vivo analysis of mtDNA replication defects in yeast. Methods 2010; 51: 426–36.

Calvo SE, Compton AG, Hershman SG, Lim SC, Lieber DS, Tucker EJ, et al. Molecular diagnosis of infantile mitochondrial disease with targeted next-generation sequencing. Sci Transl Med 2012; 4: 118ra10.

Cui TZ, Smith PM, Fox JL, Khalimonchuk O, Winge DR. Late-stage maturation of the Rieske Fe/S protein: Mzm1 stabilizes Rip1 but does not facilitate its translocation by the AAA ATPase Bcs1. Mol Cell Biol 2012; 32: 4400–9.

de Lonlay P, Valnot I, Barrientos A, Gorbatyuk M, Tzagoloff A, Taanman JW, et al. A mutant mitochondrial respiratory chain assembly protein causes complex III deficiency in patients with tubulopathy, encephalopathy and liver failure. Nat Genet 2001; 29: 57–60.

De Meirleir L, Seneca S, Damis E, Sepulchre B, Hoorens A, Gerlo E, et al. Clinical and diagnostic characteristics of complex III deficiency due to mutations in the BCS1L gene. Am J Med Genet A 2003; 121: 126–31.

Elstner M, Andreoli C, Ahting U, Tetko I, Klopstock T, Meitinger T, et al. MitoP2: an integrative tool for the analysis of the mitochondrial proteome. Mol Biotechnol 2008; 40: 306–15.

Fernández-Vizarra E, Zeviani M. Nuclear gene mutations as the cause of mitochondrial complex III deficiency. Front Genet 2015; 6: 134.

Gaignard P, Menezes M, Schiff M, Bayot A, Rak M, Ogier de Baulny H, et al. Mutations in CYC1, encoding cytochrome c1 subunit of respiratory chain complex III, cause insulin-responsive hyperglycemia. Am J Hum Genet 2013; 93: 384–9.

Ghezzi D, Arzuffi P, Zordan M, Da Re C, Lamperti C, Benna C, et al. Mutations in TTC19 cause mitochondrial complex III deficiency and

neurological impairment in humans and flies. Nat Genet 2011; 43: 259–63.
Goffrini P, Ercolino T, Panizza E, Giachè V, Cavone L, Chiarugi A, et al. Functional study in a yeast model of a novel succinate dehydrogenase subunit B gene germline missense mutation (C191Y) diagnosed in a patient affected by a glomus tumor. Hum Mol Genet 2009; 18: 1860–8.
Graham LA, Brandt U, Trumpower BL. Protease maturation of the Rieske iron-sulphur protein after its insertion into the mitochondrial cytochrome bc1 complex of Saccharomyces cerevisiae. Biochem Soc Trans 1994; 22: 188–91.
Haut S, Brivet M, Touati G, Rustin P, Lebon S, Garcia-Cazorla A, et al. A deletion in the human QP-C gene causes a complex III deficiency resulting in hypoglycaemia and lactic acidosis. Hum Genet 2003; 113: 118–22.
Invernizzi F, Tigano M, Dallabona C, Donnini C, Ferrero I, Cremonte M, et al. A homozygous mutation in LYRM7/MZM1L associated with early onset encephalopathy, lactic acidosis, and severe reduction of mitochondrial complex III activity. Hum Mutat 2013; 34: 1619–22.
Iwata S, Lee JW, Okada K, Lee JK, Iwata M, Rasmussen B, et al. Complete structure of the 11-subunit bovine mitochondrial cytochrome bc1 complex. Science 1998; 281: 64–71.
Kevelam SH, Rodenburg RJ, Wolf NI, Ferreira P, Lunsing RJ, Nijtmans LG, et al. NUBPL mutations in patients with complex I deficiency and a distinct MRI pattern. Neurology 2013; 80: 1577–83.
Koch J, Freisinger P, Feichtinger RG, Zimmermann FA, Rauscher C, Wagentristl HP, et al. Mutations in TTC19: expanding the molecular, clinical and biochemical phenotype. Orphanet J Rare Dis 2015; 10: 40.
Melchionda L, Haack TB, Hardy S, Abbink TE, Fernandez-Vizarra E, Lamantea E, et al. Mutations in APOPT1, encoding a mitochondrial protein, cause cavitating leukoencephalopathy with cytochrome c oxidase deficiency. Am J Hum Genet 2014; 95: 315–25.
Miyake N, Yano S, Sakai C, Hatakeyama H, Matsushima Y, Shiina M, et al. Mitochondrial complex III deficiency caused by a homozygous UQCRC2 mutation presenting with neonatal-onset recurrent metabolic decompensation. Hum Mutat 2013; 34: 446–52.
Morató L, Bertini E, Verrigni D, Ardissone A, Ruiz M, Ferrer I, et al. Mitochondrial dysfunction in central nervous system white matter disorders. Glia 2014; 62: 1878–94.
Nijtmans LG, Henderson NS, Holt IJ. Blue Native electrophoresis to study mitochondrial and other protein complexes. Methods 2002; 26: 327–34.
Nogueira C, Barros J, Sá MJ, Azevedo L, Taipa R, Torraco A, et al. Novel TTC19 mutation in a family with severe psychiatric manifestations and complex III deficiency. Neurogenetics 2013; 14: 153–60.
Sánchez E, Lobo T, Fox JL, Zeviani M, Winge DR, Fernández-Vizarra E. LYRM7/MZM1L is a UQCRFS1 chaperone involved in the last steps of mitochondrial Complex III assembly in human cells. Biochim Biophys Acta 2013; 1827: 285–93.
Schägger H, Link TA, Engel WD, von Jagow G. Isolation of the eleven protein subunits of the bc1 complex from beef heart. Methods Enzymol 1986; 126: 224–37.
Scheper GC, van der Klok T, van Andel RJ, van Berkel CG, Sissler M, Smet J, et al. Mitochondrial aspartyl-tRNA synthetase deficiency causes leukoencephalopathy with brain stem and spinal cord involvement and lactate elevation. Nat Genet 2007; 39: 534–9.
Schiestl RH, Gietz RD. High efficiency transformation of intact yeast cells using single stranded nucleic acids as a carrier. Curr Genet 1989; 16: 339–46.
Smith PM, Fox JL, Winge DR. Biogenesis of the cytochrome bc(1) complex and role of assembly factors. Biochim Biophys Acta 2012; 1817: 276–86.
Soto IC, Fontanesi F, Valledor M, Horn D, Singh R, Barrientos A, et al. Synthesis of cytochrome c oxidase subunit 1 is translationally downregulated in the absence of functional F1F0-ATP synthase. Biochim Biophys Acta 2009; 1793: 1776–86.
Steenweg ME, Ghezzi D, Haack T, Abbink TE, Martinelli D, van Berkel CG, et al. Leukoencephalopathy with thalamus and brainstem involvement and high lactate 'LTBL' caused by EARS2 mutations. Brain 2012; 135: 1387–94.
van der Knaap MS, Breiter SN, Naidu S, Hart AA, Valk J. Defining and categorizing leukoencephalopathies of unknown origin: MR imaging approach. Radiology 1999; 213: 121–33.
van der Knaap MS and Valk J. Magnetic Resonance of Myelination and Myelin Disorders. 2005; Ed Springer-Verlag Berlin Heidelberg.
Wortmann SB, Koolen DA, Smeitink JA, van den Heuvel L, Rodenburg RJ. Whole exome sequencing of suspected mitochondrial patients in clinical practice. J Inherit Metab Dis 2015; 38: 437–43.